# A MODEL FOR THE ULTRASONIC SCATTERING FROM MULTI-BRANCHED CRACKS

J. D. Achenbach, K.-Y. Hu and A. N. Norris*

Department of Civil Engineering
Northwestern University
Evanston, IL 60201

and

T. A. Gray and R. B. Thompson
Ames Laboratory, USDOE
Iowa State University
Ames, IA 50011

## INTRODUCTION

The ultrasonic detection (discrimination from geometrical reflectors) and sizing of intergranular stress corrosion cracks (IGSCC's) is an essential element in the continued safe operation of nuclear power plants. Unfortunately, these ultrasonic tests are rendered difficult by the complex topography of the cracks, which may include multiple facets and branches which scatter ultrasound in a nearly independent fashion. Thus, the waveforms reflected from such flaws exhibit complex shapes which may not be related to the overall extent of the flaw in a simple fashion.

As a first step towards developing a model for detection and sizing of IGSCC's, this paper presents a theory for the ultrasonic scattering from multibranched cracks. The two essential elements of the model, an elastodynamic Kirchhoff approximation for the scattering from the crack branches and a scalar Gaussian beam theory for the transducer radiation patterns, are self-consistently combined through the use of the electromechanical reciprocity relation. The resulting expressions are specialized to the case of 45° SV wave illumination of "Y" shaped, surface breaking cracks in thick plates. Interrogation is from the opposite side of the plate from the crack, as incommonly practiced angle beam inspections. The central crack branch is perpendicular to the plate surface and the end branches have variable inclinations. All branch lengths are variable and the transducer can be translated along a line perpendicular to the central branch. Using this theory, two commonly employed techniques for sizing IGSCC's, the dB drop and tip diffraction

*Now at Exxon Corporate Research Laboratory, Clinton, NJ 08801

techniques, are studied. Numerical evaluations of performance capabilities and limits are presented as a function of crack geometry.

## GENERAL FORMALISM AND ILLUMINATING FIELDS

For a crack which is free of surface tractions, the formula derived by Auld (1) for the electrical reflection coefficient reduces to

$$\delta\Gamma = \frac{i\omega}{4P} \int_{A^+} \Delta u_i \tau_{ij}^{tr} n_j \, dA, \tag{1}$$

where $A^+$ is the illuminated face of the crack, and a time-harmonic variation of the form $\exp(-i\omega t)$ has been assumed. Also, $P \equiv$ electrical power incident on the transducer, $\tau_{ij}^{tr} \equiv$ stress fields induced by the transducer in the absence of a crack, $n_j \equiv$ components of inward directed normal to A, and $\Delta u_i$ is the crack-opening displacement induced by the transducer field:

$$\Delta u_i = u_i^+ - u_i^-. \tag{2}$$

The geometrical configuration of transducer and specimen is shown in Fig. 1. The parameters (with their numerical values) are defined as follows: $2a = 1.27$ cm $\equiv$ width of the transducer, $v_o = 0.15 \times 10^6$ cm/s $\equiv$ longitudinal wave speed in the wedge, $C_T = 0.30 \times 10^6$ cm/s $\equiv$ transverse wave speed in the solid, $\Lambda_o = 2\pi v_o/\omega \equiv$ wavelength in wedge, $\Lambda_T = 2\pi C_T/\omega \equiv$ wavelength in solid, $\theta_1 = 45° \equiv$ angle of propagation in solid, $\theta_o = 20.705°$ (from Snell's law) $\equiv$ angle of propagation in wedge, $z_o = 0.635$ cm $\equiv$ axial propagation distance in wedge, $z_1 =$ variable $\equiv$ axial propagation distance in solid, $f = \omega/2\pi = 2.25$ MHz $\equiv$ frequency, $H = 2.54$ cm $\equiv$ wall thickness of plate.

In the description of the transducer field we follow the model proposed by Thompson and Lopes (2,3), which assumes that the beam profile is Gaussian in all cross-sectional planes. In this model the transverse displacement takes the form

$$u^{tr} = U_o T_{01} A e^{-i\phi} e^{i(k_o z_o + k_1 z_1)} e^{-x^2/w^2} e^{ik_T x^2/2R_c}, \tag{3}$$

where

$U_o \equiv$ constant amplitude factor, $R_c \equiv$ beam phase curvature, $\phi \equiv$ phase angle of beam, $A \equiv$ amplitude function, $w \equiv$ beam half-width, $T_{01} \equiv$ interface transmission coefficient, $k_o \equiv 2\pi/\Lambda_o, k_T = 2\pi/\Lambda_T \equiv$ wavenumbers. The functions $R_c, \phi, A$ and $w$ can be expressed in terms of a single complex quantity q, which varies linearly with propagation distance in a manner prescribed elsewhere (2,3). The axial coordinate z and, hence, q vary over a reflecting surface. The corresponding

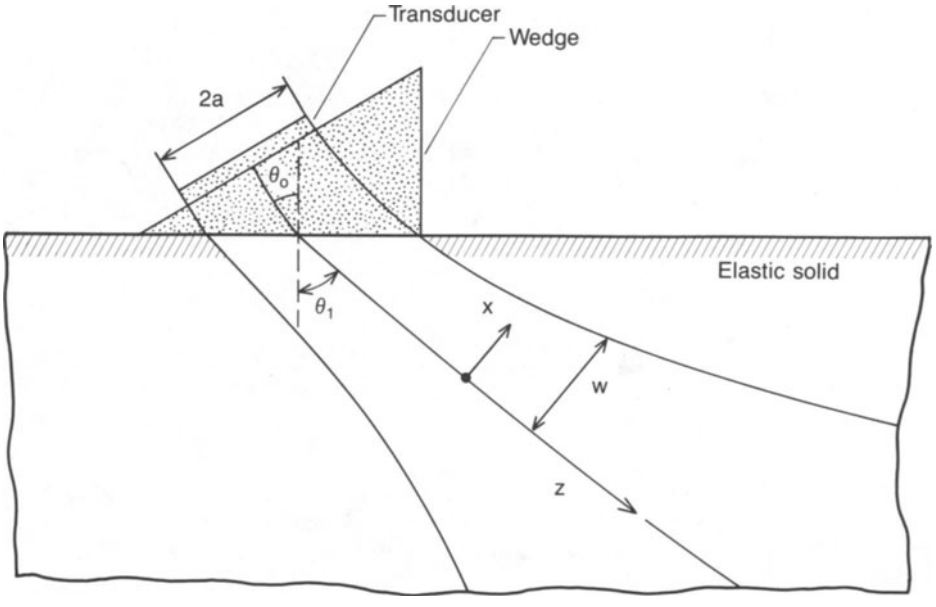


Fig. 1. Transducer, wedge and angle beam geometry.

changes in $R_c$,w,$\phi$ and A are, however, never more than a few percentage points. In the calculations these changes are neglected, and we take the values corresponding to the $z_1$ coordinate of the geometrical center of the reflecting surface. Over each flat segment the incident wave is treated as a plane wave.

## THE KIRCHHOFF APPROXIMATION

The crack-opening displacement is the unknown quantity in Eq. (1). In the Kirchhoff approximation an expression is assumed for $\Delta u_j$. It is assumed that the field on an illuminated crack face is locally the same as on an infinite traction-free plane, while on a shadow side the field is assumed to vanish. Then

$$\Delta u_j = u_j^i + u_j^r, \tag{4}$$

that is, the crack-opening displacement is taken as the sum of the incident and reflected wave on the illuminated crack face. The geometry of a reflecting surface is shown in Fig. 2a. Note that the $x_1$ axis is taken along the reflector. The incident transverse wave is defined by Eq. (3). For the purpose of computing the field on the reflector, the incident wave at the point of reflection is locally approximated by a plane wave. Then, the usual formulas for the reflection coefficients of plane waves apply (4). At a point of reflection defined by the coordinate $x_1$, the incident transverse wave is defined by

$$\underset{\sim}{u}^T = U_T(x_1)\underset{\sim}{d}^T \exp(ik_T \underset{\sim}{p}^T \cdot \underset{\sim}{x}) \tag{5}$$

where $\underset{\sim}{d}^T$ defines the direction of particle displacement, $\underset{\sim}{p}^T$ is the propagation vector, and $k_\alpha = \omega/c_\alpha$, $\alpha$=L,T, with $C_L$ and $C_T$ being the propagation velocities of longitudinal and transverse waves. An explicit formula for $U_T(x_1)$ will be given in the sequel.

The reflected field is defined as

$$\underset{\sim}{u}^{T\beta} = R_\beta^T U_T(x_1)\underset{\sim}{d} \exp(ik_\beta \underset{\sim}{p}^\gamma \cdot \underset{\sim}{x}) \tag{6}$$

where $R_\beta^T$ is the reflection coefficient. The index $\beta$ defines the type of the reflected wave. We have $\beta$ = L or T. The index $\gamma$ is defined as $\gamma = r\beta$. $\underset{\sim}{d}^\alpha$ and $\underset{\sim}{p}^\alpha$ define the directions of particle displacement and wave propagation, respectively, for these reflected wave types. The angles $\theta_L$ and $\theta_T$, as defined in Fig. 2a, are related by Snell's law

$$\sin\theta_L = \kappa \sin\theta_T \ , \ \kappa = C_L/C_T. \tag{7}$$

It is noted that there is a critical angle $\theta_T = \theta_{cr} = \sin^{-1}(1/\kappa)$ beyond which the left hand side of Eq. (7) becomes larger than unity, and hence $\theta_L$ becomes imaginary.

The total displacement on the reflecting surface, which is written as $\Delta u$, may now be expressed as

$$\underset{\sim}{\Delta u} = U_T(x_1)(\underset{\sim}{d}^T + R_L^T \underset{\sim}{d}^{rL} + R_T^T \underset{\sim}{d}^{rT}) \exp(ik_T p_1^T x_1) \tag{8}$$

It remains to determine an expression for the amplitude factor $U_T(x_1)$, for the various reflecting elements of the crack. This has been done by evaluating Eq. (3), after the appropriate propagation distance, at the geometrical center of the individual reflecting surfaces. The geometry of the crack and the incident rays is shown in Fig. 2b. The crack has a main stem of depth d and two branches of lengths b. The left and right branches make angles with the vertical line of the main stem of magnitudes $\theta_\ell - \pi/2$ and $\pi/2 - \theta_r$, respectively. The stem length, branch length, and branch angles are all variables. The right branch is illuminated only by the main beam, ray (a). The left branch and the main stem are illuminated not only by the main beam, rays (b) and (c), but also by the beam reflected from the lower face of the plate, rays (d) and (e). The contributions of each of the illumination processes are summed to obtain the total scattering solution.

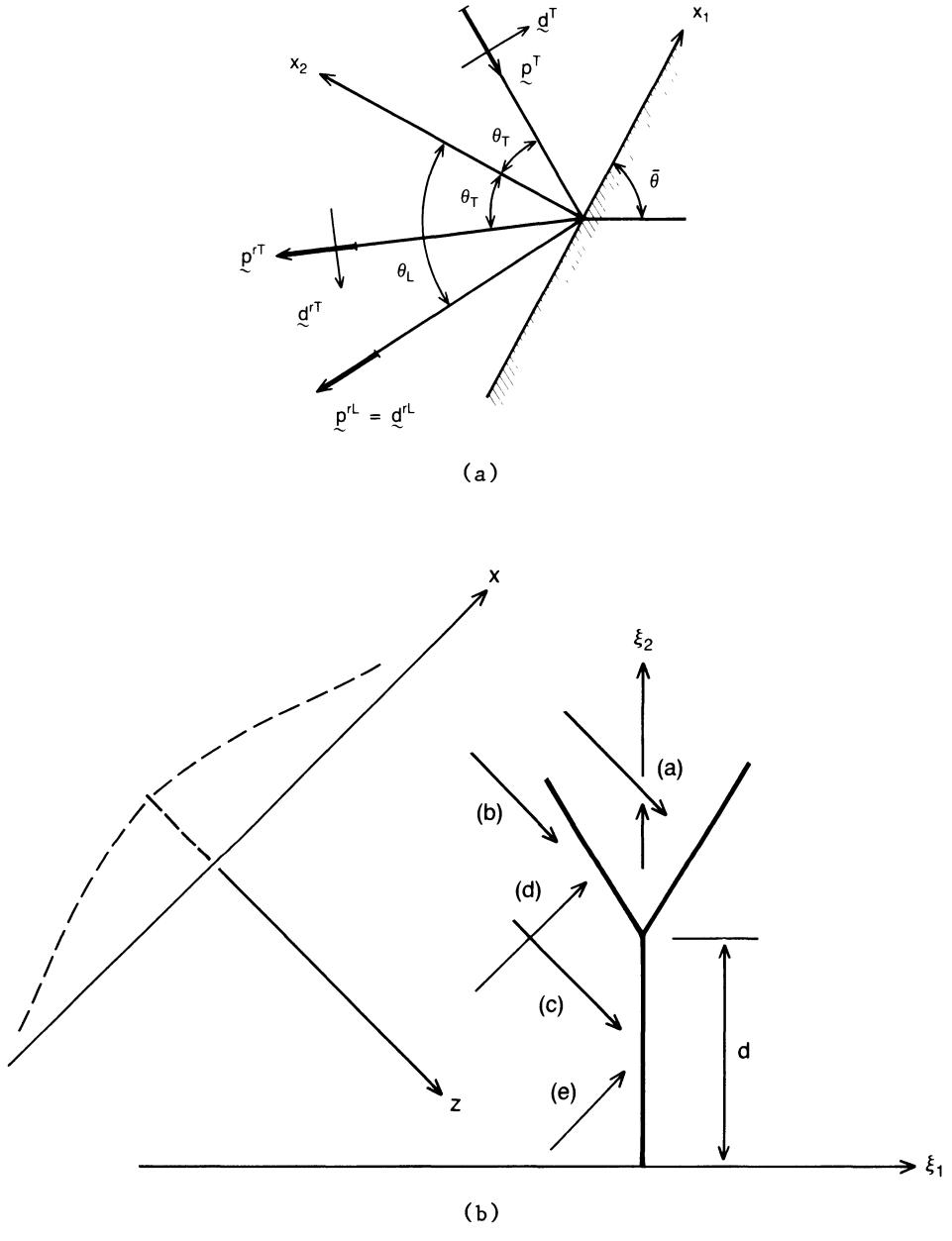


Fig. 2. a) Geometry of a reflecting surface, b) illumination of main stem and branches.

STRESS FIELD PRODUCED BY THE TRANSDUCER

It follows from Eqs. (3) and (5) that the displacement field generated by the transducer may be written in the general form

$$\underset{\sim}{u}^{tr} = U_o T_{o1} W(x) \underset{\sim}{d}_T \exp(ik_T \underset{\sim}{p}^T \cdot \underset{\sim}{x}) \ , \tag{9}$$

where W(x) is a weight factor in the xz-systems:

$$W(x) = U_T(x_1)/U_o T_{o1} \ , \tag{10}$$

which locally adjusts the plane wave $U_o T_{o1} \underset{\sim}{d}_T \exp(ik_T \underset{\sim}{p}^T \cdot \underset{\sim}{x})$.

The stress field $\tau_{ij}^{tr}$ is the stress field corresponding to Eq. (9). In computing the components we will, however, introduce the simplification that only the plane wave part of Eq. (9) will be substituted in Hooke's law. Thus,

$$\tau_{ij}^{tr} = U_o T_{o1} W(x) \tau_{ij}^{pw} \ , \tag{11}$$

where $\tau_{ij}^{pw}$ are the stress components corresponding to the plane wave $\underset{\sim}{d}_T \exp(ik_T \underset{\sim}{p}^T \cdot \underset{\sim}{x})$. It is noted that each stress component has two parts, corresponding to the direct incident wave (ray cases, a,b,c), and the reflection from the lower face of the plate (ray cases d and e), respectively.

NUMERICAL EXAMPLES OF BASIC THEORY

We start by rewriting Eq. (1) in dimensionless form:

$$\frac{H}{U_o T_{o1}} \frac{P\delta\Gamma}{\mu_o U_o T_{o1} c_T} = i \frac{k_T}{4} \frac{H}{d} \int_{L^+} \frac{\Delta u_i}{U_o T_{o1}} \frac{\tau_{ij}^{tr} d}{\mu_o U_o T_{o1}} n_j d\ell \tag{12}$$

where in the present two-dimensional geometry $L^+$ defines the line segments which represent the illuminated crack faces. Also, H ≡ thickness of plate, d ≡ depth of main stem of the crack. The integrations defined by Eq. (12) have been carried out in the local coordinates $x_1, x_2$ of each reflector. A simplification has been introduced in the expressions for $\Delta u_i$ and $\tau_{ij}^{tr}$, in that the weight factor W(x), which enters in Eq. (9) and subsequently in Eq. (11), has been taken as a constant whose value is equal to W(x) evaluated at the geometrical center, $x = x_c$, of the particular reflector. This simplifies the integrations in Eq. (12) significantly. Since the beam does not tend to vary greatly over an individual reflector (a branch, or the main stem of the crack) the accuracy of the computations is not significantly affected. The values of $W(x_c)$ will remain different for the different reflectors that form the branched stress-corrosion crack.

Numerical results have been obtained for $\bar{\theta}_\ell = 120°$, $\bar{\theta}_r = 60°$, $b/d = 0.6$, $d/H = 0.098$, $H = 2.54$ cm, $\bar{x}/d = 0$, $\bar{z}/d = 14.4$. Figure 3 shows the dimensionless electric signal as it is observed by the transducer, due to backscattering. The plotted amplitudes are defined as

$$|\delta\Gamma| = \left| \frac{H}{U_o T_{o1}} \quad \frac{P\delta\Gamma}{\mu U_o T_{o1} c_T} \right| \tag{13}$$

The position of the mouth, M, of the crack is defined by coordinates $\bar{x}$ and $\bar{z}$. Thus, the position of the beam relative to the crack can be varied by variation of $\bar{x}$. The corresponding variation of $\bar{z}$ follows from the relation $\bar{z} = H\sqrt{2} + \bar{x}$. Thus, translation of the transducer will affect the backscattered field.

The frequency s

The frequency spectrum of the total superimposed backscattered signal for all ray systems has been plotted in Fig. 3 for several selected values of $\bar{x}$. It is noted that the amplitude decreases as $|\bar{x}|$ increases. The difference between equal positive and negative values of $\bar{x}$ is too small to be noted on the scale of Fig. 3. The results show what will be observed when the transducer is moved over the top-surface of the plate.

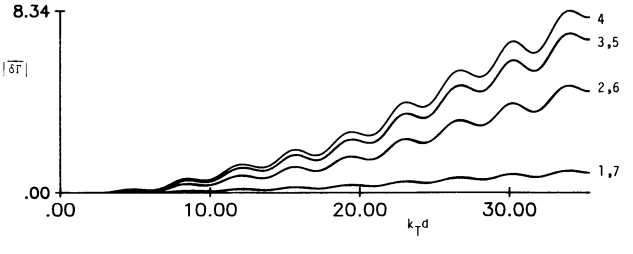


Fig. 3. $|\overline{\delta\Gamma}|$ versus $k_T d$; 1:$\bar{x}$=-1.0; 2:$\bar{x}$=-.5; 3:$\bar{x}$=-.25; 4:$\bar{x}$=0.0; 5:$\bar{x}$=0.25; 6:$\bar{x}$=.5; 7:$\bar{x}$=1.0.

## COMPUTATION OF SYNTHETIC EXPERIMENTAL DATA

In order to simulate ultrasonic scattered signals from IGSCC's such as might be obtained in practice, this model must be further convolved with an appropriate "reference" signal which is representative of typical ultrasonic transducers. For the results to follow, a reference waveform consisting of a corner reflection from a steel sample using a 45° incident shear wave was used. This signal was obtained by Ms. Janet Wade of the EPRI NDE Center using a 2.25 MHz

broadband transducer. The video signal which would be produced by the rectification of this r.f. signal was then simulated by computing the envelope of the analytical signal (see Ref. 5 for details).

By way of example, Fig. 4 shows a particular IGSCC configuration and the resulting video signal obtained from the model. In this computation, the crack stem and branches were 0.25 cm in length with a 60° angle separating the branches, as shown in part (a). The transducer was assumed to be 0.25 in. (0.685 cm) in radius and positioned so that its central axis was directed at the crack mouth. Five scattering events contribute to the signal shown in Fig. (4b). The corresponding ray paths and signal features are labeled as (i)...(v) in this figure in their order of arrival times. First, ray path (i) consists of the backscattered tip-diffracted signal from the left branch. This is of small relative amplitude since illumination and scattering are nearly at edge-on incidence in this case. The second event, labeled (ii), is the backscattered signal from the right branch. This is larger than feature (i) since illumination and scattering are more nearly specular. Ray path (iii) consists of illumination of the left branch after one reflection from the free surface and then scattering directly back to the transducer, as shown, and simultaneously the reverse path. The fourth, and largest feature, is the corner reflection from the crack mouth, labeled as (iv) in Fig. 4b. Finally, the fifth feature consists of illumination of the left branch by a wave which reflects from the free surface and whose scattered rays subsequently reflect again from the free surface before arriving at the transducer. A critical feature of the IGSCC model is its incorporation of transducer radiation patterns which allows the effects of probe motion to be predicted. Examples of this were shown in Fig. 3 in which spectra were computed for different transducer positions relative to an IGSCC. In the time domain, the spectral differences correspond to changes in the arrival times and amplitude of the five signals shown in Fig. 4b. The simulations of the dB drop and crack-tip sizing capabilities which follow are based upon the ability to predict these changes.

## ANALYSIS OF THE dB DROP AND TIP DIFFRACTION SIZING TECHNIQUES

Two techniques for estimating the depth of an IGSCC via ultrasonic indications have been analyzed. In the dB-drop technique, the depth estimate is obtained by first positioning the interrogating transducer to obtain the peak amplitude from an IGSCC and then moving the transducer to each side of the crack until the amplitude has been reduced by a nominal amount. The -3dB level has been selected in this work.

The IGSCC model was exercised in order to test the dB-drop technique against synthetic waveforms in two "heats". In the first heat, a 2.50 MHz center frequency transducer of 1/4" radius was used to interrogate defects of total depth h = 0.125", 0.25", 0.5", 0.75", 0.90". Recall that the plate thickness was taken to be 1" in all cases. For each depth h, the ratio d/h of crack stem length to total depth was varied as d/h = 0.5, 0.75, 0.90, 0.99 and the angle $\theta$ between branches assumed values of 0°, 30°, 60°, 90°. Results of all trials in this heat are shown in Fig. 5, which plots true vs estimated depth. For these simulations, the estimated depth was taken to be just the distance over which the transducer was moved to define the -3dB points. All size estimates were essentially

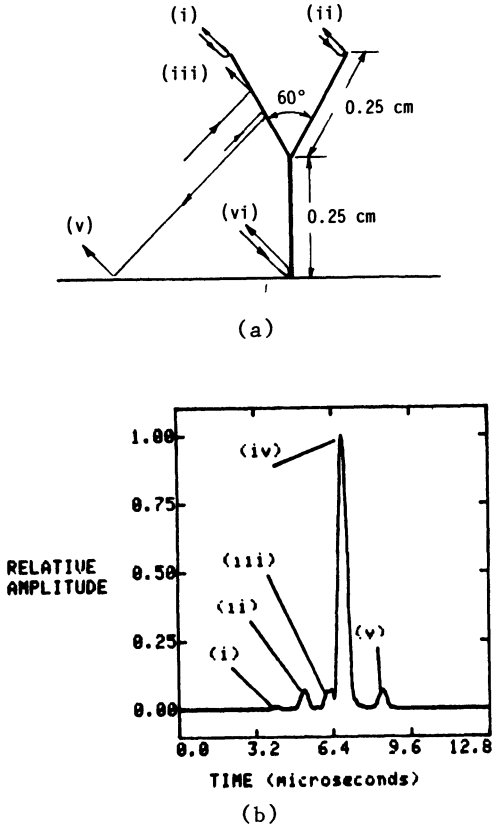


Fig. 4. Sample computation. a) crack geometry, b) envelope of signal when central ray strikes crack mouth.

the same and are indistinguishable on the scale of this figure. This lack of correlation arises because the predominant feature in the IGSCC waveforms (cf. Fig. 4) was the corner reflection at the crack mouth. Thus, the dB-drop points were indicative primarily of the passage of the illuminating ultrasonic beam profile past the crack mouth as the transducer was translated along the top surface of the plate. No reliable size information can be gleaned in this manner.

For the second heat, the transducer radius and frequency were varied for a given crack shape. In particular, two transducer radii,

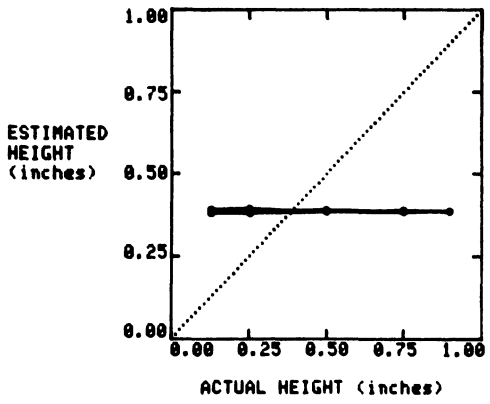


Fig. 5. True versus estimated heights for dB-drop technique applied to "Heat 1".

0.125" and 0.25", and two center frequencies, 2.5 MHz and 1.25 MHz, were chosen for IGSCC's having d/h = 0.9 and $\theta = 60°$. The same range of depths h were chosen. No transducer radius or frequency exhibited any meaningful sizing capability. The perceived size merely reflected the interrogating ultrasonic beam profile. All of these results confirm the experimental observation (6) that the dB-drop technique does not give reliable estimates of IGSCC depth.

The second IGSCC sizing method addressed in the model simulations is the pulse arrival time (PAT) technique. This method utilizes the fact that the ultrasonic indications from the mouth and the tip of an IGSCC, which are detected at different transit times, are simply related to the depth of an IGSCC. In principle, the PAT method can give highly accurate estimates of IGSCC depth, although there are some practical limitations. The most significant such limitation is the weakly scattering property of the IGSCC crack tips. In practical situations, where IGSCC's occur near welds, the weak nature of tip diffraction coupled with ultrasonic noise and scattering from the weld material can cause the tip-diffracted signal to be unresolvable. Such phenomena are beyond the scope of this study and the results to be presented are based upon the assumption that the tip-diffracted signals from an IGSCC can be clearly identified.

The PAT method was applied to the IGSCC parameters described previously as the first "heat". Thus, the overall depth h, the ratio of stem length to depth, d/h, and the angle between branches, $\theta$, were varied. In all cases, the branches were of equal length and positioned symmetrically with respect to the crack stem. In accordance with standard PAT practices, the transducer was first positioned to produce the maximum signal amplitude which corresponds

to the corner reflection. The transducer was then translated until the maximum amplitude of any signal component occurring at an earlier time than the corner signal was obtained. The time delay $\Delta t$ between the peak corner signal and the peak early arrival was recorded. This time delay is proportional to the depth h of the IGSCC via the easily derived formula

$$h = \frac{C_T \Delta t}{2\sqrt{2}} \tag{14}$$

where the factor $\sqrt{2}$ is particular to 45° interrogation.

Figure 6 illustrates the use of the PAT technique to size IGSCC's for the branch angles $\theta = 30°$. The diagonal dashed line corresponds to perfect sizing, i.e., $h_{TRUE} = h_{est}$, and the estimated values are indicated by circles. The ratio, d/h, of stem length to total depth was varied as d/h = 0.5, 0.75, 0.90, 0.99. The fact that different estimates of h are obtained for different values of d/h is a result of the simplifying assumptions used in the IGSCC model. In all cases the estimated height approaches the true height as d/h→1.

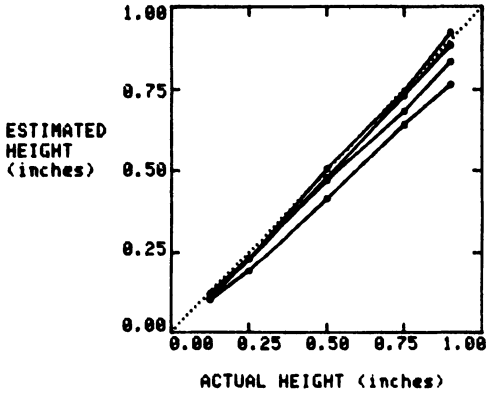


Fig. 6. True versus estimated heights for PAT technique with 30° interbranch spacing.

Similar results were calculated for $\theta = 0°$, 60°, and 90°, and accurate sizing results were obtained in the majority of cases. However, when the angle between branches was $\theta = 90°$, the method failed when d/h = 0.5 for all depth h and for d/h = 0.75 and 0.90

when h = 0.75" and 0.9". For those cases, the largest amplitude feature in the simulated waveforms corresponded to reflection from the right branch (path (ii) in Fig. 4b). This would thus be mistaken for the "mouth" signal. This ray path corresponds to the shortest transit time among the scattered signals from the various facets of the IGSCC model, and so it was not possible to obtain an earlier arriving signal. (Note that the IGSCC model computes zero scattering from the left branch in this crack geometry since the Kirchhoff approximation which was used to define the scattering phenomena predicts zero scattering at edge-on incidence.) Since such a configuration of IGSCC facets might plausibly occur in reality, the PAT would be expected to give erroneous results in this case.

## CONCLUSIONS

A model for the ultrasonic scattering from a Y-shaped IGSCC has been formulated and used to simulate the performance of the dB-drop and tip diffraction techniques. The former is found to be deficient in that it primarily provides a measure of beam profile rather than crack depth. The latter generally gives accurate sizing results, although a few anomalous cases have been identified. These results are consistent with recent experimental sizing results obtained on EDM notches (6).

In the calculation, the illuminating and receiving radiation patterns were locally treated as plane waves over each stem or branch of the crack to simplify integration. However, the basic formulae derived do not depend on this assumption. Replacement of the local plane wave approximation by numerical integration would produce some quantitative change in the results but would not substantially alter these conclusions.

## ACKNOWLEDGEMENT

This work was sponsored by the Electric Power Research Institute under research project RP2405-5.

## REFERENCES

1. B. A. Auld, Wave Motion, 1, 3-10 (1979).
2. R. B. Thompson and E. F. Lopes, "The effects of focussing and refraction on Gaussian ultrasonic beams", Journal of Nondestructive Evaluation (in press).
3. R. B. Thompson and E. F. Lopes, "Relationship of Gaussian beam theory to scanned ultrasonic measurements with commercial transducers", this proceedings.
4. J. D. Achenbach, Wave Propagation in Elastic Solids, (North-Holland, Amsterdam, 1973).
5. T. A. Gray and R. B. Thompson, "Model calculations of the variation of ALN features with the parameters of an IGSCC", Report of the Committee on Physics Review of the Adaptive Learning Network Methodology, Report NP3216 (Electric Power Research Institute, Palo Alto, 1983).
6. Gary Dau and Mohamad Behravesh, "Status of IGSCC sizing", in, Effective Nondestructive Examination for Prssurized Components, R. Nichols and G. J. Dau, Eds. (Applied Science Publishes, in press).